2025 International Conference on Intelligent Computing
July 26-29, Ningbo, China
https://www.ic-icc.cn/2025/index.php

Change Detection in Wide-Field Video Images Based on Low Illumination Enhancement

Jia He, Tianyu Ren, Yankai Cao, Zhenhong Jia(✉), and Sensen Song

College of Computer Science and Technology, Xinjiang University,
Urumqi 830046, China
jzhh @xju.edu.cn

Abstract. In low illumination environments, the image quality of eagle- eye surveillance devices is significantly degraded by high-density random noise and inhomogeneous illumination. In addition, the change targets in the surveillance area are usually small, which further increases the difficulty of change detection (CD), and is prone to false positives and negatives. In this paper, we propose a new unsupervised CD method for small targets. Specifically, under low illumination, the image is pre enhanced using the bright channel prior and Single-Scale Retinex (SSR) algorithm to improve image quality; two difference images (DIs) are generated by the arctangent operator and the Chi-Square Transform (CST), and the difference information is fused using the improved multiplicative fusion (MTF) technique to ensure the completeness of the details in the change region and suppress the noise. Particularly, for areas with few changes or no changes, we propose a threshold segmentation method based on Log-Normal Distribution Histogram Fitting Error Minimization (LNDFEM) to achieve the segmentation of change regions. Experimental results demonstrate that the proposed method outperforms comparison algorithms in terms of overall error, F1-Score, and Kappa coefficient, and exhibits stronger robustness.

Keywords: Low Illumination Change Detection, Wide Field of View, Security Surveillance, Log-normal Distribution, Image Enhancement.

1 Introduction

Change detection (CD) technology is widely used in remote sensing, security monitoring, urban planning, and other fields, playing a crucial role in decision-making and resource management. In low-light conditions, the primary task is to detect subtle changes between multi-temporal video frames captured by the Eagle Eye visual sensor. Due to the wide field of view and insufficient illumination in Eagle Eye surveillance, image quality deteriorates, leading to an increased risk of false positives and missed detections, which adversely impacts the precision and efficiency of monitoring systems [1]. Therefore, developing a small-target CD method that is adapted to low-light environments is essential to enhancing the performance of monitoring systems in complex scenarios. This study aims to propose a novel CD technique for low-light conditions to improve monitoring efficiency and accuracy in such environments.

Change detection technology is classified into supervised and unsupervised methods based on whether it relies on ground truth annotation data. Supervised methods depend on manually labeled data for processing, which is labor-intensive and time-consuming [2]. Therefore, unsupervised CD methods have been developed in the literature [3]. The process of unsupervised CD typically involves three steps: 1) preprocessing; 2) Difference Image (DI) extraction; and 3) DI binarization. Currently, there is limited research on CD for low-light, wide-field video images with preprocessing enhancement, with most studies focusing on image enhancement[4] and denoising[5] under low-light conditions, such as methods based on joint filtering[6], the Retinex model[7], and deep learning approaches[8]. However, these methods have limitations in noise handling and illumination balancing, making them difficult to fully meet the needs of low-light surveillance.

Methods for extracting change information from DIs include clustering and thresholding techniques. However, clustering algorithms exhibit significant limitations in low-light or noisy environments. They are often sensitive to the selection of initial parameters, noise, and outliers. For example, unsupervised algorithms like k-means and hierarchical clustering can lead to misclassification and unstable detection results in low-light or noisy scenarios. Thresholding algorithms, such as the Otsu[9] algorithm, Expectation-Maximization (EM)[10] algorithm, and Kittler-Illingworth (KI)[11] threshold selection algorithm, generally rely on the significant statistical probability of changed pixels, ensuring that the change class can be modeled in the histogram of the difference image. This guarantees the reliability and accuracy of the threshold selection. However, under low-light, wide-field conditions, where the number of changed pixels is very small or even nonexistent, existing thresholding algorithms are prone to failure.

To address the above issues, this paper proposes an image enhancement method based on the bright channel prior and Single-Scale Retinex (SSR) algorithm, and utilizes the Log-Normal Distribution Histogram Fitting Error Minimization (LNDFEM) method for unsupervised CD.

The main innovations of this work can be summarized as follows:

- A preprocessing enhancement method combining the bright channel prior and SSR algorithm is proposed, effectively improving the low visibility and removing noise in the image.
- To improve the fusion accuracy of the DI, a threshold-based multiplicative fusion technique is introduced, significantly enhancing the quality of the DI.
- An unsupervised thresholding method based on LNDFEM is proposed. This method is suitable for images with few change pixels and no-change scenes under wide-field conditions, improving detection accuracy and robustness.

2 Method

2.1 Overview

As shown in **Fig. 1**, for the video images captured by surveillance devices under low-light conditions, two frames T1 and T2 of the same scene at different times are extracted

for CD. In this section, we first introduce the preprocessing of low illumination image, then describe the generation of difference image, and finally generate change detection image based on log-normal distribution histogram fitting error minimization.

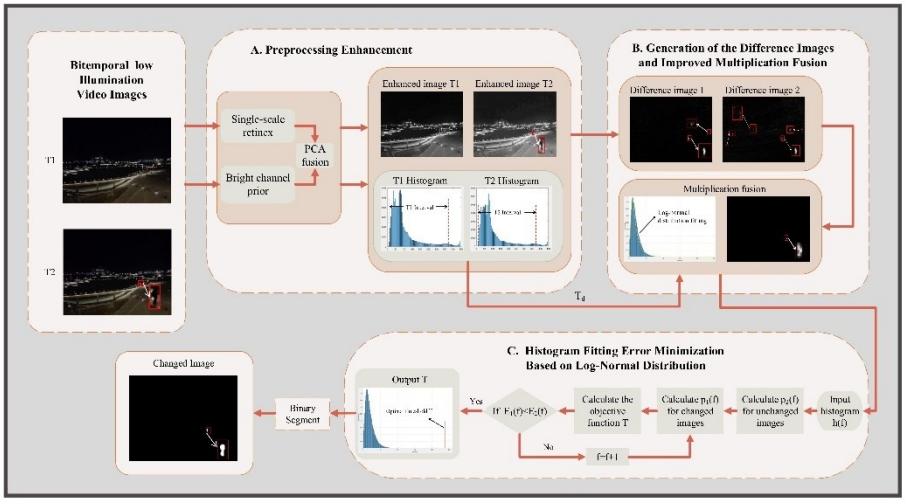

Fig. 1. Flowchart of the proposed method.

2.2 Preprocessing Enhancement

Enhancement can improve the visibility of an image while preserving its visual naturalness. The traditional SSR algorithm uses the center-surround theory to estimate the illumination map, which leads to blurred image edges. Therefore, a globally adaptive illumination map [12] is used instead of Gaussian filtering to obtain the reflection component $R(x, y)$, where $L_w(x, y)$ represents the brightness value of the low-light image, $L_g(x, y)$ represents the globally adaptive brightness value, and σ is a small positive constant. The formula is as follows:

$$R(x, y) = log\left(\frac{L_w(x, y)}{L_g(x, y)} + \sigma\right) \tag{1}$$

Inspired by the dark channel prior dehazing method [13], experimental observations show that the bright channel prior theory is also applicable to low-light images. This theory suggests that in most areas, at least one color channel has a high intensity. Therefore, the bright channel image under low light can be expressed by the following formula:

$$I_{light}(x) = \max_{y \in \Omega(x)} \left(\max_{c \in \{R,G,B\}} \left(I_c(y) \right) \right) \tag{2}$$

where I_c represents the image of a particular color channel of image I; $\Omega(x)$ represents the local region centered at pixel x, $\max_{y\in\Omega(x)}$ indicating the region maximum value filtering.

After performing SSR enhancement on the low-light image, it is fused with the bright channel image using Principal Component Analysis (PCA) to improve the quality of the enhanced image.

2.3 Generation of the Difference Images and Improved Multiplication Fusion

The logarithmic operator performs well in handling high brightness changes but has issues with numerical stability and accurately reflecting real change trends. The mean ratio excels at enhancing the contours of change areas and preventing information loss, but it may introduce noise and affect the preservation of details. The extreme pixel ratio operator [14] has advantages in suppressing background information and enhancing change area information, but it is overly sensitive to changes in small pixel values.

To overcome these limitations, this study adopts an improved arctangent operator to generate DI. The arctangent operator can compress difference values when pixel differences are large, preventing excessive amplification of differences, balancing the differences in high dynamic range images, and smoothing abrupt changes in the image, thereby reducing sharp jumps in the difference map. The formula is as follows:

$$DI_1(x,y) = \left|\arctan\left(\frac{(I_2(x,y) - I_1(x,y) + 1)}{(I_2(x,y) + I_1(x,y) + 1)}\right)\right|^{mse} \tag{3}$$

where the Mean Squared Error (mse) adaptively adjusts the sensitivity to differences in different regions, ensuring that the response in high-change areas is not overly drastic, while low-change areas remain sensitive.

Furthermore, the Chi-Square Transformation (CST) effectively distinguishes actual changes from random noise when generating the DI by leveraging its statistical properties. It quantifies significant changes in pixel intensity, providing an accurate measure of change for each pixel. The robustness of CST reduces the influence of non-change factors such as lighting and shadows, while its sensitivity to outliers enhances the ability to identify changing objects. Therefore, using CST to generate the DI is an effective strategy. The principle of CST is based on Mahalanobis Distance, and the calculation formula is as follows:

$$DI_2(x,y) = \sqrt{\sum_{k=1}^{K}\left(\frac{DI_{1_k}(x,y) - \mu_k}{\sigma_k}\right)^2} \tag{4}$$

where K is the number of color channels, $DI_{1_k}(x,y)$ is the difference value in the k-th channel at pixel (x,y), μ_k is the mean of the k-th channel difference image, and σ_k is the standard deviation of the k-th channel difference image.

The change information provided by a single difference image is still affected by residual noise. Although the multiscale transform method[14,15,16] can improve the

accuracy of CD, it often introduces redundant decompositions, leading to detail loss and increased computational complexity.

To further improve the quality of the DI, an improved multiplicative fusion (MTF) technique is proposed by combining the advantages of CST and the arctangent operator. The formula is as follows:

$$F = \begin{cases} \dfrac{DI_1 * DI_2}{\max(DI_2)}, & |I_2(x,y) - I_1(x,y)| \geq T_d \\ DI_2, & |I_2(x,y) - I_1(x,y)| < T_d \end{cases} \quad (5)$$

where T_d represents the threshold for possible changes in the image. If T_d is set too large, some pixels that may change will not be MTF. Conversely, if T_d is set too small, some unchanged pixels will be mistakenly detected as changed pixels. Specifically, when T_d equals 0, the improved fusion method is equivalent to MTF.

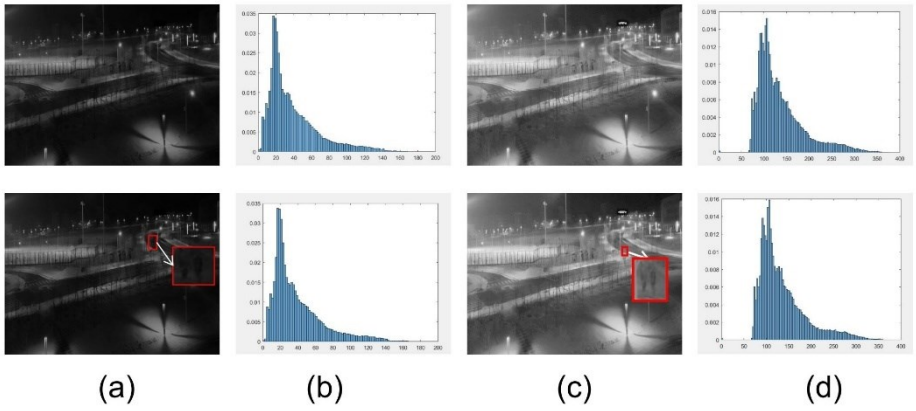

Fig. 2. Pre-enhancement and histogram diagram (a) Original gray image, (b) Histogram of (a), (c) Enhance image, (d) Histogram of (c).

For the issue of determining the optimal threshold T_d, this paper proposes an approximation method based on the log-normal distribution to obtain the value of T_d. Since the grayscale distribution of low-light images after pre-enhancement approximately follows a log-normal distribution, as shown in **Fig. 2**, we can significantly reduce the computational complexity of determining T_d by utilizing this probabilistic statistical property. Let $\overline{m}_i$, $\overline{\sigma}_i$ (i = 1,2) represent the statistical mean and standard deviation of the two frames I_1 and I_2, respectively. The interval $\overline{m}_i - \overline{\sigma}_i, \overline{m}_i - 3\overline{\sigma}_i$ denotes the partial sample set of the two frames I_1 and I_2, and then T_d is defined as:

$$T_d = 0.5\left[\left(max(\overline{m}_1 + 3\overline{\sigma}_1, \overline{m}_2 + 3\overline{\sigma}_2) - min(|\overline{m}_1 - \overline{\sigma}_1|, |\overline{m}_2 - \overline{\sigma}_2|)\right) + 0\right] \quad (6)$$

where $\left(max(\overline{m}_1 + 3\overline{\sigma}_1, \overline{m}_2 + 3\overline{\sigma}_2) - min(|\overline{m}_1 - \overline{\sigma}_1|, |\overline{m}_2 - \overline{\sigma}_2|)\right)$ is the maximum possible grayscale difference between the partial sample sets of the two frames, and 0 is the minimum possible grayscale difference. Thus, T_d is approximately the average

grayscale difference between these two partial sample sets. In most cases, the defined interval contains more than half of the pixels in each frame, so T_d can be approximated as the threshold for possible changes across the entire image.

2.4 Histogram Fitting Error Minimization Based on Log-Normal Distribution

Inspired by Histogram Fitting Error Minimization [14], LNDFEM is derived under the assumption that the pixel values in the DI are independent, with the unchanged class approximately following a log-normal distribution and the changed class following a Gaussian distribution. Let $p(f|\omega_u)$ represent the conditional probability density function (PDF) of unchanged pixels in the DI, and $p(f|\omega_c)$ represent the conditional PDF of changed pixels in the DI. σ_c and $\sigma_u$represent the weights of the changed and unchanged classes, respectively. Therefore, $p(f|\omega_u)$ and $p(f|\omega_c)$ are defined as follows:

$$\begin{aligned} p(f|\omega_u) &= \frac{1}{f\sigma_u\sqrt{2\pi}}\exp\left(-\frac{(\ln f-\mu_u)^2}{2\sigma_u^2}\right), f>0 \\ p(f|\omega_c) &= \frac{1}{\sqrt{2\pi}\sigma_c}\exp\left(-\frac{(f-\mu_c)^2}{2\sigma_c^2}\right) \end{aligned} \tag{7}$$

where σ_u represents the standard deviation of unchanged pixels, σ_c represents the standard deviation of changed pixels, μ_u represents the mean of unchanged pixels, and μ_c represents the mean of changed pixels.

Finally, according to the law of total probability, the PDF of the DI can be modeled as a mixture density distribution consisting of two density components associated with ω_c and ω_u. There are two cases: the first case is when there are changes in the multi-temporal images, and the second case is when there are no changes. Therefore, let $p_1(f)$ and $p_2(f)$ represent the PDFs in these two cases, respectively. If there are changes in the multi-temporal images, $p_1(f)$ can be expressed as:

$$p_1(f) = p(f|\omega_u)P(\omega_u) + p(f|\omega_c)P(\omega_c), f \in (0,255] \tag{8}$$

where $P(\omega_u)$ and $P(\omega_c)$ represent the prior probabilities of the unchanged class and the changed class, respectively.

If there is no change in the multi-temporal images, the PDF of the DI follows a log-normal distribution. The expression for $p_2(f)$ is:

$$p_2(f) = \frac{1}{f\sigma\sqrt{2\pi}}\exp\left(-\frac{(\ln f-\mu)^2}{2\sigma^2}\right), f>0 \tag{9}$$

where μ represents the mean of all pixels and σ represents the standard deviation of all pixels.

The objective function used in this method is to minimize the histogram fitting error, where $h(f)$ represents the histogram of the DI.

$$E_1(f) = \min_f \sum_{f=1}^{255}\left(p_1(f)-h(f)\right)^2 \tag{10}$$

According to the Bayesian minimum error criterion (maximum posterior probability criterion), that is:

$$\begin{aligned}\hat{\omega} &= \arg \max_{\omega=[\omega_u,\omega_c]} p(\omega|f) \\ &= \arg \max_{\omega=[\omega_u,\omega_c]} (p(f|\omega)p(\omega))\end{aligned} \tag{11}$$

To minimize the error probability, each pixel in DI should be assigned to the class with the maximum posterior conditional probability, that is:

$$\begin{cases} p(\omega_c|f) > p(\omega_u|f), & f > T \\ p(\omega_c|f) \le p(\omega_u|f), & f \le T \end{cases} \tag{12}$$

To find the optimal threshold T, that is, when $f = T$, $p(\omega_c|f) = p(\omega_u|f)$, we conclude that:

$$\frac{P(\omega_c)}{P(\omega_u)} = \frac{p(f|\omega_u)}{p(f|\omega_c)} \tag{13}$$

If there are changes in the multi-temporal images, the fitting of $p_1(f)$ should be better than that of $p_2(f)$. The optimized fitting criterion is defined as follows:

$$\sum_{f=1}^{255}(p_1(f) - h(f))^2 < \sum_{f=1}^{255}(p_2(f) - h(f))^2 \tag{14}$$

In summary, our objective function is to minimize the fitting error under the conditions of equations (13) and (14). Therefore, the optimization model for solving the threshold T is defined as:

$$\begin{aligned} T &= \arg \min_{f} \sum_{f=1}^{255}(p_1(f) - h(f))^2 \\ \text{s.t.} &\left| \frac{P(\omega_c)}{P(\omega_u)} - \frac{p(f \mid \omega_u)}{p(f \mid \omega_c)} \right| < t \\ &\sum_{f=1}^{255}(p_1(f) - h(f))^2 < \sum_{f=1}^{255}(p_2(f) - h(f))^2 \end{aligned} \tag{15}$$

where the parameter t is a positive number with a relatively small absolute value. The parameters in equations (7) to (9) are estimated using equation group (16):

$$
\begin{aligned}
P(\omega_u) &= \sum_{f=1}^{T} h(f), \\
P(\omega_c) &= 1 - P(\omega_u), \\
\mu &= \sum_{f=1}^{255} h(f)\ln f, \\
\sigma^2 &= \sum_{f=1}^{255} h(f)(\ln f - \mu)^2, \\
\mu_u &= \frac{1}{P(\omega_u)} \sum_{f=1}^{T} h(f)\ln f, \\
\sigma_u^2 &= \frac{1}{P(\omega_u)} \sum_{f=1}^{T} h(f)(\ln f - \mu_u)^2, \\
\mu_c &= \frac{1}{P(\omega_c)} \sum_{f=T+1}^{255} h(f) f, \\
\sigma_c^2 &= \frac{1}{P(\omega_c)} \sum_{f=T+1}^{255} h(f)(f - \mu_c)^2.
\end{aligned}
\tag{16}
$$

3 Experiments

3.1 Dataset and Evaluation Metrics

The scarcity of low-light wide-field video image datasets is mainly due to the challenges of data acquisition and annotation under complex illumination and diverse noise in real-world scenes. This significantly limits existing datasets and results in a lack of resources for change detection under low-light conditions.

To address this, we have constructed the Low-Light Wide-Field (LLWF) dataset, which includes 11 types of monitoring scenes such as building entrances, campus roads, and parking lots. Each scene contains video footage lasting 3–10 minutes with a resolution of 4096×1800. Representative frames are extracted from the original videos, resulting in 84 pairs of high-quality images and corresponding reference images. To minimize registration errors and avoid illumination variation interference, all image pairs are registered and downsampled to 500×380 pixels. Based on scene complexity, the dataset is divided into simple and complex scenes. Some representative scenes are shown in **Fig. 3**. The LLWF dataset features small targets, varying target sizes, and diverse noise types, providing ample testing and validation conditions for change detection algorithms in low-light wide-field environments. It helps comprehensively evaluate the robustness and accuracy of algorithms in complex scenarios, leading to more precise change detection results.

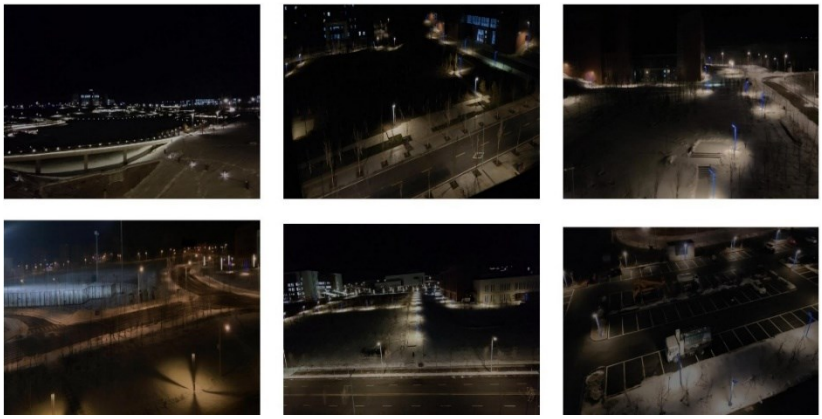

Fig. 3. LLWF dataset.

To evaluate the performance of the algorithm, two quantitative metrics from the receiver operating characteristic (ROC) curve were employed to assess the quality of DI: the area under the curve (AUC) and the diagonal distance (Ddist) [18]. Higher values of these metrics indicate better detection performance. The objective evaluation metrics for CD results include overall error (OE), percentage correct classification (PCC), kappa coefficient, and F1-Score.

3.2 Comparison Experiment

To demonstrate the effectiveness of the proposed methods, we selected eight methods for comparison on the LLWF dataset, including OKC_AF[14], NPSG [19], MSF_NF [20], INLPG[21], CWNN[22], ASEA[23], IRG-MCS[24] and AGSCC [18]. The experimental results were also analyzed by subjective and objective indicators.

3.3 Performance Analysis of Different Methods for Generating Difference Image

We conducted experiments on six datasets from different scenes, calculated the average evaluation metrics, and compared the quality of difference images generated by PCA[25], EWF[20] and ADEL[14] fusion methods with those generated by our proposed MTF. As shown in **Table 1**, our method outperforms the others in terms of AUC and Ddist, indicating superior performance of the difference images generated by our approach.

Table 1. Quantitative Criteria AUC and Ddist for Different Fusion Methods.

Method	$\overline{AUC}$	$\overline{Ddist}$
PCA	0.9892	1.3538
EWF	0.9880	1.3495
ADEL	0.9810	1.3426
MTF	**0.9963**	**1.3745**

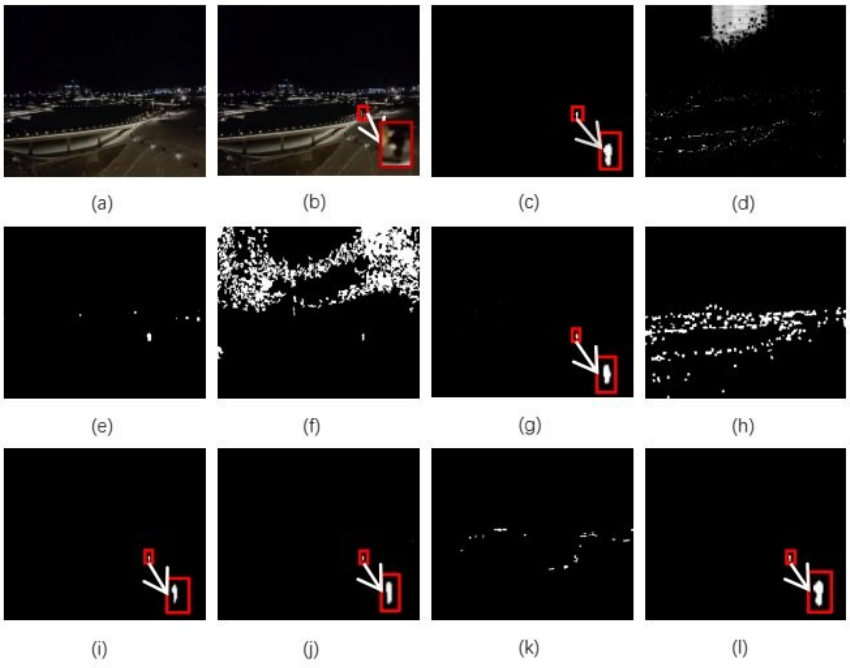

Fig. 4. Objective Evaluation Indexes of Experimental.

3.4 Accuracy Analysis of Change Detection Algorithms

As shown in **Fig. 4**, our results are closer to the reference image, indicating a lower false alarm rate compared to other methods. Additionally, methods like NPSG, CWNN, IRG-MCS, AGSCC, and INLPG, which did not take measures to suppress high-density random noise under low-light conditions, resulted in numerous false change points in the unchanged regions. ASEA, MSF_NF, and OKC_AF effectively overcome the noise impact but, to some extent, expand the range of the valid change areas. Our method, similar to MSF_NF and OKC_AF in its framework, improves the image contrast through preprocessing enhancement, followed by the use of an improved MTF to generate high-quality DI, effectively suppressing noise. Traditional binarization processing lacks robustness in regions with minimal pixel changes. LNDFEM takes the overall probability distribution into account and compares the histogram fitting errors of $p_1(f)$ and $p_2(f)$. In cases with no change or minimal changes, the histogram fitting error of $p_2(f)$ is smaller than that of $p_1(f)$, which drives the optimal threshold to gradually increase until the optimization model satisfies the constraints. According to the evaluation metrics in **Table 2**, our method outperforms other algorithms in terms of Kappa coefficient, F1-Score, and PCC.

Table 2. Objective Evaluation Indexes of Experimental

Algorthms	OE	PCC	Kappa	F1-Score
NPSG	7302	0.9615	0.0109	0.0113
INLPG	320	0.9983	0.2076	0.2079
CWNN	11539	0.9392	0.0102	0.0109
ASEA	35	0.9998	0.6601	0.6601
IRG-MCS	8001	0.9578	0.0092	0.0096
MSF_NF	18	0.9999	0.7999	0.8000
OKC_AF	11	0.9999	0.8533	0.8533
AGSCC	599	0.9968	0.0651	0.0655
Proposed	**6**	0.9999	**0.9318**	**0.9318**

Table 3. Indicators of Average Evaluation of Experimental Data

Agorthms	$\overline{OE}$	$\overline{PCC}$	$\overline{Kappa}$	$\overline{\mathrm{F1-Score}}$
NPSG	3482.4	0.9644	0.1197	0.0913
INLPG	153.1	0.9992	0.3529	0.3530
CWNN	24410.3	0.8715	0.0066	0.0086
ASEA	29982.7	0.8422	0.1973	0.1975
IRG-MCS	8001	0.9603	0.0071	0.0075
MSF_NF	16.5	0.9999	0.5583	0.5583
OKC_AF	9.2	0.9999	0.8130	0.8130
AGSCC	1097.5	0.9943	0.0326	0.0328
Proposed	**5.1**	0.9999	**0.9135**	**0.9135**

Table 4. Average Evaluation Metrics of Detection Results for Unchanged Scenes

Algorthms	NPSG	INLPG	ASEA	IRG-MCS	OKC_AF	Proposed
$\overline{OE}$	1517.4	3665.6	51330.3	8191.1	6	**1**
$\overline{PCC}$	0.9920	0.9807	0.7300	0.9569	0.9999	0.9999

3.5 Analysis of Change Detection Methods

To demonstrate the stability and robustness of the algorithm, we selected 84 sets of different change scenarios from the LLWF dataset for multi-temporal video image pairs and conducted experiments with our method and the comparison methods. The average CD results are shown in **Table 3**. The results indicate that our algorithm outperforms the other algorithms in terms of Kappa coefficient and F1-Score, achieving an increase of at least 12.30% compared to other methods, and a decrease in OE of at least 44.57%.

Especially under low-light and wide-field conditions, our method meets the CD requirements, showcasing outstanding performance advantages.

For the unchanged scenes, we selected 15 different scene datasets for experiments to assess the stability of the algorithm. The average evaluation metrics of the experimental results are listed in **Table 4**. The data shows the lowest OE value, indicating that the proposed algorithm demonstrates superior robustness in no-change scenarios, effectively reducing the occurrence of false detections.

4 Conclusion

In this paper, a novel CD method for monitoring video images in low-light, wide-field conditions with subtle or no changes is proposed. First, multi-temporal monitoring images are enhanced using a combination of the bright channel prior and SSR. Then, an improved multiplicative fusion method is applied, leveraging the complementary information from adaptive arctangent ratio and CST. Finally, the fused DI is classified using the histogram fitting error minimization method based on log-normal distribution to accurately extract change areas. Experimental results show that the proposed algorithm effectively detects subtle changes in low-light environments and outperforms existing comparison algorithms in terms of accuracy and robustness, demonstrating superior detection performance and noise resistance.

Acknowledgments. This work was supported by the National Natural Science Foundation of China (No.62261053), the Tianshan Talent Training Project-Xinjiang Science and Technology Innovation Team Program (2023TSYCTD0012), and the China Postdoctoral Science Foundation (Certificate Number: 2024M752692).

References

1. Jianing Wang, Xiaodong Wang, and Yunhui Li. Stray light nonuniform background elimination method based on image block self-adaptive gray-scale morphology for wide-field surveillance. Applied Sciences, 12(14):7299, 2022.
2. Xinzheng Zhang, Hang Su, Ce Zhang, Xiaowei Gu, Xiaoheng Tan, and Peter M. Atkinson. Robust unsupervised small area change detection from sar imagery using deep learning. ISPRS Journal of Photogrammetry and Remote Sensing, 173:79–94, 2021.
3. Yakoub Bazi, Lorenzo Bruzzone, and Farid Melgani. An unsupervised approach based on the generalized gaussian model to automatic change detection in multitemporal sar images. IEEE Transactions on Geoscience and Remote Sensing, 43(4):874–887, 2005.
4. Shijie Hao, Xu Han, Yanrong Guo, Xin Xu, and Meng Wang. Low-light image enhancement with semi-decoupled decomposition. IEEE Transactions on Multi- media, 22(12):3025–3038, 2020.
5. Qian Ma, Yao Wang, and Tieyong Zeng. Retinex-based variational framework for low-light image enhancement and denoising. IEEE Transactions on Multimedia, 25:5580–5588, 2022.

6. Jiangxin Dong, Jinshan Pan, Jimmy S. Ren, Jinhui Tang, Liang Lin, and Ming- Hsuan Yang. Learning spatially variant linear representation models for joint filtering. IEEE Transactions on Pattern Analysis and Machine Intelligence,44(11):8355–8370, 2021.
7. Jun Xu, Yingkun Hou, Dongwei Ren, Li Liu, Fan Zhu, Mengyang Yu, Haoqian Wang, and Ling Shao. Star: A structure and texture aware retinex model. IEEE Transactions on Image Processing, 29:5022–5037, 2020.
8. Li-Wen Wang, Zhi-Song Liu, Wan-Chi Siu, and Daniel PK Lun. Lightening net- work for low-light image enhancement. IEEE Transactions on Image Processing, 29:7984–7996, 2020.
9. Sudipan Saha, Francesca Bovolo, and Lorenzo Bruzzone. Unsupervised deep change vector analysis for multiple-change detection in vhr images. IEEE Transactions on Geoscience and Remote Sensing, 57(6):3677–3693, 2019.
10. Lorenzo Bruzzone and Diego Fernàndez Prieto. Automatic analysis of the difference image for unsupervised change detection. IEEE Transactions on Geoscience and Remote Sensing, 38(3):1171–1182, 2000.
11. Guo Wang, Yao Wang, and Lihua Jiao. Adaptive spatial neighborhood analysis and rayleigh-gauss distribution fitting for change detection in multi-temporal remote sensing images. Journal of Remote Sensing, 13(4):631–638, 2009.
12. Hyunchan Ahn, Byungjik Keum, Daehoon Kim, and Hwang Soo Lee. Adaptive local tone mapping based on retinex for high dynamic range images. In 2013 IEEE International Conference on Consumer Electronics (ICCE), pages 153–156. IEEE, 2013.
13. Kaiming He, Jian Sun, and Xiaoou Tang. Single image haze removal using dark channel prior. IEEE Transactions on Pattern Analysis and Machine Intelligence, 33(12):2341–2353, 2011.
14. Baoqiang Shi, Zhenhong Jia, Jie Yang, and Nikola K. Kasabov. Unsupervised change detection in wide-field video images under low illumination. IEEE Transactions on Circuits and Systems for Video Technology, 33(4):1564–1576, 2023.
15. Wenhua Zhang, Licheng Jiao, Fang Liu, Shuyuan Yang, and Jia Liu. Adaptive contourlet fusion clustering for sar image change detection. IEEE Transactions on Image Processing, 31:2295–2308, 2022.
16. Peng Chen, Zhenhong Jia, Jie Yang, and Jia Liu. Unsupervised change detection of sar images based on an improved nsst algorithm. Journal of the Indian Society of Remote Sensing, 46(4):631–638, 2018.
17. Kaiyu Zhang, Xiaolei Lv, Huiming Chai, and Jingchuan Yao. Unsupervised sar image change detection for few changed area based on histogram fitting error minimization. IEEE Transactions on Geoscience and Remote Sensing, 60:1–19, 2022.
18. Y. Sun, L. Lei, D. Guan, et al. Image regression with structure cycle consistency for heterogeneous change detection. IEEE Transactions on Neural Networks and Learning Systems, 35(2):1613–1627, 2024.
19. Yuli Sun, Lin Lei, Xiao Li, Hao Sun, and Gangyao Kuang. Nonlocal patch similarity based heterogeneous remote sensing change detection. Pattern Recognition,109:107598, 2021.
20. Yong Zhu, Zhenhong Jia, Jie Yang, and Nik Kasabov. Change detection in multitemporal monitoring images under low illumination. IEEE Access, 8:126700– 126712, 2020.
21. Yuli Sun, Lin Lei, Xiao Li, Xue Tan, and Gangyao Kuang. Structure consistency- based graph for unsupervised change detection with homogeneous and heterogeneous remote sensing images. IEEE Transactions on Geoscience and Remote Sensing, 60:1–21, 2021.
22. Feng Gao, Xiaoyan Wang, Yujie Gao, and Jun Liu. Sea ice change detection in sar images based on convolutional-wavelet neural networks. IEEE Geoscience and Remote Sensing Letters, 16(8):1240–1244, 2019.

23. Z. Lv, F. J. Wang, T. Liu, et al. Novel automatic approach for land cover change detection by using vhr remote sensing images. IEEE Geoscience and Remote Sensing Letters, 19:1–5, 2021.
24. Y. Sun, L. Lei, D. Guan, et al. Iterative robust graph for unsupervised change detection of heterogeneous remote sensing images. IEEE Transactions on Image Processing, 30:6277–6291, 2021.
25. L. Li, H. Ma, X. Zhang, et al. Synthetic aperture radar image change detection based on principal analysis and two-level clustering. Remote Sensing, 16(11):1861, 2024.